Using Coordinate Transformation of Navier-Stokes Equations To Solve Flow In Multiple Helical Geometries

A. N. Cookson[a], D. J. Doorly[a], S. J. Sherwin[a,*]

[a]*Department of Aeronautics, Imperial College London, Prince Consort Road, London, SW7 2AZ, UK*

Abstract

Recent research on small amplitude helical pipes for use as bypass grafts and arterio-venous shunts, suggest that mixing may help prevent occlusion by thrombosis. It is proposed here that joining together two helical geometries of different helical radii will enhance mixing with only a small increase in pressure loss. To determine the velocity field, a coordinate transformation of the Navier-Stokes equations is used, which are then solved using a 2-D high-order mesh combined with a Fourier decomposition in the periodic direction. The results show that the resultant velocity fields in each component geometry differ strongly from the corresponding solution for a single helical geometry. The results suggest that although the mixing behaviour will be weaker than an idealised prediction suggests, it will be improved from that generated in a single helical geometries.

Key words:

1. Introduction

1.1. Motivation

Approximately 30,000 coronary artery bypass graft procedures are performed each year in the UK according to the British Heart Foundation, however over 50% of the grafts fail within 10 years due to the development of neo-intimal hyperplasia [1]. Similarly, arterio-venous shunts, constructed from ePTFE, which are used for vascular access during dialysis, are prone to occlusion by thrombosis and intimal hyperplasia. In the United States alone there are 175,000 ePTFE grafts used for permanent vascular access, with the 1 and 2-year primary patency rates currently at 50% and 25% respectively. Consequently, much research has been conducted in the past few decades to design grafts that will remain patent for far longer, ideally matching the life-span of the patient.

A promising new idea is to construct the grafts from small amplitude helical pipes [2]. In preliminary *in-vivo* trials, and subsequently a preliminary clinical study [3], the degree of thrombotic occlusion was reduced in the helical grafts, compared with standard grafts. In-plane mixing was hypothesised to be responsible, and a computational investigation was performed to understand and quantify the mixing effect in these devices [4]. The results of that work lead to the idea that mixing in grafts can be enhanced by appropriate combinations of helical geometries, with only small additional pressure losses.

1.2. Flow in helical pipes

A helix is a three-dimensional space curve that can be described by the parametric equations:

$$x = R\cos t, \tag{1}$$
$$y = R\sin t, \tag{2}$$
$$z = ct, t \in (0, 2\pi\}, \tag{3}$$

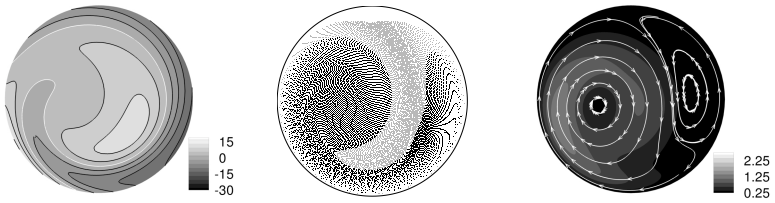
*Corresponding author: s.sherwin@imperial.ac.uk

where R is the radius or amplitude of the helix and c is a constant parameter, such that the wavelength or one pitch of the helix equals $2\pi c$. For a helical pipe the internal radius is an additional parameter $D/2$. A very brief summary of the results for single helical geometries, shown in [4], is given to provide context for the motivation of the work, and also to aid understanding of the results for the combined helical geometry. A Reynolds number of 250, defined as $\frac{\overline{w}D}{\nu}$, was used, to match representative physiological conditions in a bypass graft. For all the geometries the pitch length was fixed at $6D$, and the the helical radius varied from $0.1D$ to $0.5D$.

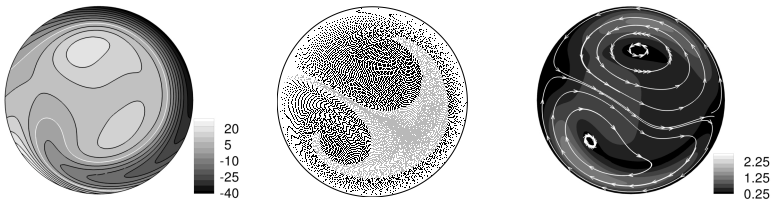
For geometries where $R < c$, the curvature of the helix increases with R. This causes the axial velocity profile to become increasingly asymmetric, and the peak velocity to move closer to the pipe wall on the inside of the bend. For all the geometries examined the secondary-flow is a single vortical structure, Figures 1(a) & 1(d), which increases in strength with R. For $R = 0.1D$ particles in the flow move in a single vortex trajectory. However, as R is increased, a second vortex emerges in the particle trajectories, Figures 1(b) & 1(e), despite only a single vortex existing in the velocity field. This apparent discrepancy can be explained by a sequence of reference frame changes or coordinate transformations. These remove the effects of the translation and rotation on the velocity field, so that the in-plane velocity field can be expressed as:

$$\mathbf{V}_{in-plane} = \mathbf{V}_{cartesian} - \mathbf{V}_{translation} - \mathbf{V}_{rotation} \tag{4}$$

Note that the angle between the dividing line of the two vortices and the vertical, also increases with R.



(a) Axial vorticity - $R = 0.2D$ (b) Particle trajectory slice (c) $\mathbf{V}_{in-plane}$



(d) Axial vorticity - $R = 0.5D$ (e) Particle trajectory slice (f) $\mathbf{V}_{in-plane}$

Figure 1: Despite a single vortical structure in the flow, a double vortex structure appears in the particle trajectories, which can be explained by determining $\mathbf{V}_{in-plane}$, Eqn. (4). Figs. (a)-(c) show results for $R = 0.2D$, and (d)-(f) for $R = 0.5D$.

1.3. Combined helical geometries

In their seminal paper [5], Jones, Thomas & Aref, show that chaotic advection [6] can be generated by concatenating 180^o curved sections of pipe, with some twist angle χ at each junction, which ranged from 0^o to 180^o. Their configuration is shown in Figure 2(a). It was assumed that a fully-developed Dean flow solution existed in each section of pipe, and that the transition between each section was instantaneous. Although they acknowledge that this is physically unrealistic, it is explained that a flow scenario similar to this can be generated experimentally, and therefore that their approach is valid.

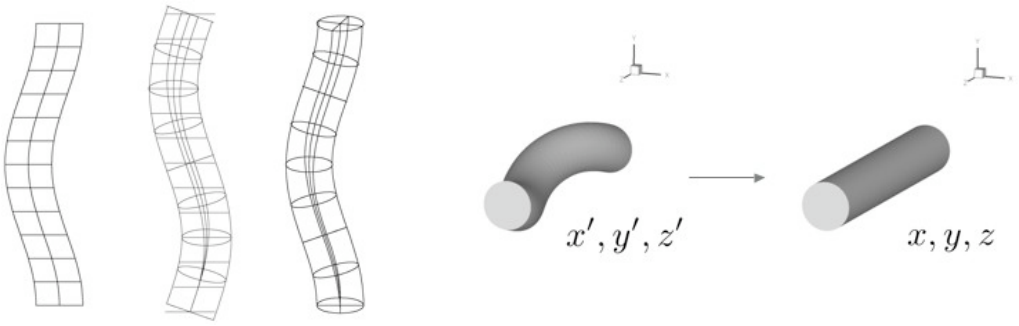
helix. Furthermore, the impact of any changes on the in-plane velocity field will be assessed, and the implications this may have on the mixing examined, although a full examination of the resultant mixing phenomenon is beyond the scope of this paper. Additionally, quantification of the persistence of the vortical structures, and the length scales over which they adjust to the changing geometry, may also provide general insight into the behaviour of the swirling flows through the multiple non-planar bends that exist in the larger arteries of the human body.

To these ends we present a method for solving the flow in combined helical pipes using a coordinate transformation of spline-fitted geometries, within a spectral/hp element framework.

2. Method

2.1. Coordinate Transformation of Navier-Stokes Equations

For the range of values of R and c under consideration, the resultant helical pipe geometry can be well approximated by a circular cross-section simply translated by a helical centreline. The validity of this approximation is illustrated in Figure 3(a). This approximation can be conceptually reversed by performing a coordinate mapping from a helical geometry to a cylindrical geometry. The mapping is then applied to the Navier-Stokes equations, which are then solved in the cylindrical domain, but with an additional body-force term which represents that applied to the flow by the original geometry. A coordinate transformation has been used previously to investigate the bluff body flows in [7] and channel flow in [8]. The mathematical details follow.



(a) Comparison of helical pipe (right) with approximation (left)

(b) Transformation of solution domain coordinate system

Figure 3: Coordinate transformation concept applied to small amplitude helical pipes

In a coordinate system (x', y', z'), the non-dimensional Navier-Stokes equations are:

$$\frac{\partial \mathbf{u}'}{\partial t'} + (\mathbf{u}' \cdot \nabla')\mathbf{u}' = -\nabla' p' + \frac{1}{R_e}\nabla'^2 \mathbf{u}' \,, \tag{5}$$

$$\nabla' \cdot \mathbf{u}' = 0 \,, \tag{6}$$

A coordinate transformation is defined, as illustrated in Figure 3(b):

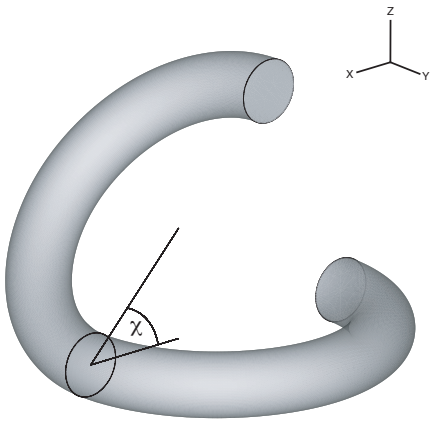
$$x = x' - \xi_x(z') \,, \tag{7}$$

$$y = y' - \xi_y(z') \,, \tag{8}$$

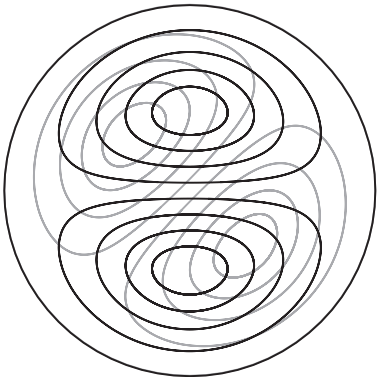
$$z = z' \,, \tag{9}$$

$$t = t' \,, \tag{10}$$

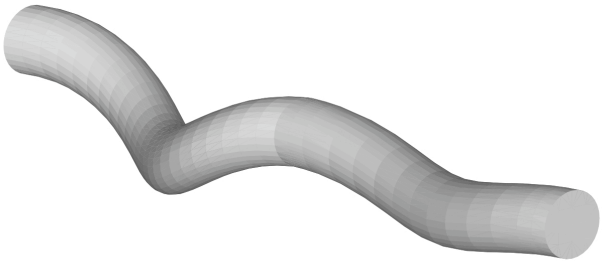
Figure 1 showed that the in-plane velocity field can be a double vortex structure with varying sizes/strengths of vortex and varying angle of vortical dividing line. A similar flow environment of streamline crossing, to that of Jones *et al*. [5], can be achieved by concatenating various helical geometries. One such example is shown in Figure 2(c) for the geometries $R = 0.25D$ and $R = 0.5D$. The corresponding in-plane streamlines are shown in Figure 2(d).



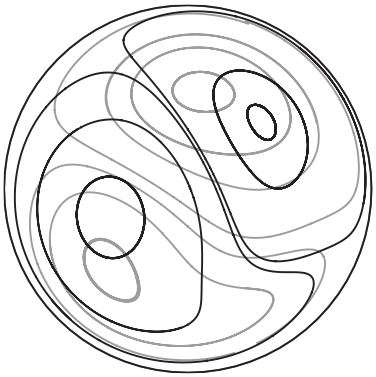
(a) Twisted pipe configuration used by Jones *et al*. for $\chi = 45^o$



(b) Dean flow streamlines crossing at 45^o



(c) A combined helical pipe geometry for $R = 0.5$ and $R = 0.25$



(d) Streamline crossing for helical pipe flows, $R = 0.5$ and $R = 0.25$

Figure 2: Demonstration of the concept of streamline crossing, which Jones *et al.* [5] found to produce excellent mixing through chaotic advection

A first approximation to the potential mixing behaviour of such a geometry can be made by simply tracking particles through the velocity of the periodic solution of $R = 0.25D$ for one pitch length, and then through the geometry $R = 0.5D$, as for the Dean flows in [5]. In fact, for the helical pipe flows this is thought to be a better approximation for the following reason. Whilst the effective in-plane flow seen by the particles is a two vortex solution, the topology of the Eulerian velocity field does not vary significantly. Transition between the two flows only requires that the strength of a single vortical structure increases/decreases slightly, and that the peak axial velocity moves closer to or further from the wall. This approximation does not required the complete reorientation of vortices as in [5].

Nevertheless, we would like to test the strength of this assumption by performing flow calculations for 'true' combined helical geometries, and comparing the velocity field within each half to that of the corresponding single

For a helix, the mapping terms $\xi_x(z')$ and $\xi_y(z')$ are simply those that define a helical centreline:

$$\xi_x(z') = R\cos(z'/c)\,, \tag{11}$$
$$\xi_y(z') = R\sin(z'/c)\,, \tag{12}$$

Using the chain rule, the partial derivative operators transform to the following:

$$\frac{\partial}{\partial x'} = \frac{\partial}{\partial x}\,, \tag{13}$$
$$\frac{\partial}{\partial y'} = \frac{\partial}{\partial y}\,, \tag{14}$$
$$\frac{\partial}{\partial z'} = \frac{\partial}{\partial z} - \frac{\partial \xi_x}{\partial z}\frac{\partial}{\partial x} - \frac{\partial \xi_y}{\partial z}\frac{\partial}{\partial y}\,, \tag{15}$$
$$\frac{\partial}{\partial t'} = \frac{\partial}{\partial t}\,, \tag{16}$$

Taking the time derivatives of Eqs. (7-9), gives transformations for velocity and pressure:

$$u = u' - w'\frac{\partial \xi_x}{\partial z}\,, \tag{17}$$
$$v = v' - w'\frac{\partial \xi_y}{\partial z}\,, \tag{18}$$
$$w = w'\,, \tag{19}$$
$$p = p'\,, \tag{20}$$

Substituting all the modified terms into Eq. (5) produces the Navier-Stokes equations in a coordinate system (x, y, z):

$$\frac{\partial \mathbf{u}}{\partial t} + (\mathbf{u}\cdot\nabla)\mathbf{u} = -\nabla p + \frac{1}{R_e}\nabla^2\mathbf{u} + \mathbf{A}(\mathbf{u}, p, \xi_x, \xi_y)\,, \tag{21}$$
$$\nabla\cdot\mathbf{u} = 0\,, \tag{22}$$

Note that the mapping is divergence free, that is, it satisfies:

$$\frac{\partial \xi_x}{\partial x} + \frac{\partial \xi_y}{\partial y} = 0 \tag{23}$$

Consequently the continuity equation is unaltered, so that:

$$\frac{\partial u'}{\partial x'} + \frac{\partial v'}{\partial y'} + \frac{\partial w'}{\partial z'} = \frac{\partial u}{\partial x} + \frac{\partial v}{\partial y} + \frac{\partial w}{\partial z} \tag{24}$$

The body force term, $\mathbf{A}(\mathbf{u}, p, \xi_x, \xi_y)$, has components A_x, A_y and A_z. For the sake of brevity, only the A_x term will be considered in detail. A_x and A_y both contain the convective derivative of the z-component of the transformed Navier-Stokes equations. Substituting this into A_x, removes the time derivative of w, producing:

$$\begin{aligned} A_x = & \left[-\frac{d\xi_x}{dz}\frac{d\xi_y}{dz}\frac{\partial p}{\partial y} - w^2\frac{d^2\xi_x}{dz^2} + \frac{d\xi_x}{dz}\frac{\partial p}{\partial z} - \left(\frac{d\xi_x}{dz}\right)^2\frac{\partial p}{\partial x}\right] \\ & + \frac{1}{R_e}\left[-2\frac{d\xi_y}{dz}\frac{\partial w}{\partial y}\frac{d^2\xi_x}{dz^2} - 2\frac{d\xi_y}{dz}\frac{\partial^2 u}{\partial y\partial z} - \frac{d^2\xi_x}{dz^2}\frac{\partial u}{\partial x} + 2\frac{d\xi_x}{dz}\frac{d\xi_y}{dz}\frac{\partial^2 u}{\partial x\partial y}\right. \\ & - 2\frac{d^2\xi_x}{dz^2}\frac{\partial w}{\partial x}\frac{d\xi_x}{dz} + \left(\frac{d\xi_y}{dz}\right)^2\frac{\partial^2 u}{\partial y^2} + 2\frac{\partial w}{\partial z}\frac{d^2\xi_x}{dz^2} - \frac{d^2\xi_y}{dz^2}\frac{\partial u}{\partial y} \\ & \left. + w\frac{d^3\xi_x}{dz^3} - 2\frac{d\xi_x}{dz}\frac{\partial^2 u}{\partial x\partial z} + \left(\frac{d\xi_x}{dz}\right)^2\frac{\partial^2 u}{\partial x^2}\right] \end{aligned} \tag{25}$$

2.2. Spline-fitted Multiple Helical Geometries

At the junction between the two different helical geometries, there is a discontinuity in the curves' gradients (and subsequent derivatives). Although this can be easily implemented within the solver, the discontinuity will be difficult for the Fourier modes to resolve, hindering the exponential convergence of the solution. Physically, such a discontinuity could also provoke undesirable flow separation at the joint, and it is unlikely that any manufactured geometry would contain such a discontinuity, particularly if constructed from ePTFE as used in medical devices.

To remove this discontinuity a spline is defined to span the transition region between the points $z/c = 7\pi/4$ and $z/c = 9\pi/4$, and pass through the point at $z/c = 2\pi$. Equation (25) shows that the body force terms include derivatives of the mappings ξ_x and ξ_y upto the 3rd order. Therefore we require that at the endpoints of the spline, the 1^{st}, 2^{nd} and 3^{rd} derivatives of the spline match those of the helical functions. This enforces a requirement for a seventh-order spline fit. A general spline function is used, which takes as arguments the radii of both geometries. These spline function coordinate mappings are then used in exactly the same way as the helical functions.

2.3. Spectral/hp element method

The cylindrical domain, with periodic boundary conditions, allows a Fourier basis expansion to be used in the axial direction z.

$$\varphi_r(\xi_3) = e^{ir\beta\xi_3},\ \beta = \frac{2\pi}{L_{\xi_3}} \tag{26}$$

For example, the velocities are stored in the following form:

$$\mathbf{v}(x, y, z, t) = \sum_{m=0}^{M-1} \mathbf{v}_m(x, y, t) e^{i\beta mz} \tag{27}$$

Taking the Fourier transform of the Navier-Stokes equations, essentially reduces the problem to m two dimensional Navier-Stokes equations:

$$\frac{\partial \mathbf{v}_m}{\partial t} = -\tilde{\nabla}_m p_m + \nu \tilde{\nabla}_m^2 \mathbf{v}_m + \widehat{[\mathbf{v} \cdot \nabla \mathbf{v}]} \quad in\ \Omega_m,\ m = 0, \ldots, M-1 \tag{28}$$

where the 'hat' signifies the Fourier transform, and the equations are solved on the M two-dimensional slices Ω_m. The linear differential operators are also modified, and are:

$$\tilde{\nabla}_m = \left(\frac{\partial}{\partial x}, \frac{\partial}{\partial y}, im\beta\right), \quad \left(\tilde{\nabla}_m^2 = \frac{\partial^2}{\partial x^2} + \frac{\partial^2}{\partial y^2} - \beta^2 m^2\right) \tag{29}$$

Within the 2-D planar mesh, high-order C_0-continuous polynomial basis functions are used, with both triangular elements and quadrilateral elements with curved boundaries. This approach has several advantages; no remeshing is required for each geometry, computational time is smaller than for a full 3-D mesh, and the overhead on parallelisation is small. Full details of the spectral/hp element method can be found in [9].

3. Results

A Reynolds number of 250 is used, in accordance with the work on single helical geometries [4], but other values are also used for completeness. The pitch is fixed at six pipe diameters ($6D$) for both geometries, again as in the previous study. The helical radius of the first geometry is designated R_A, and that of the second, R_B. Results are presented for the case $R_A = 0.2D$ and and $R_B = 0.5D$, for R_e of 125 and 250. Slices of the velocity field are taken at intervals of $z/c = \pi/2$, as shown in Figure 4.

Figures 5 and 6 show the axial velocity and vorticity results for the geometry, $R_A = 0.2$ and $R_B = 0.5$. For comparison purposes, the corresponding axial velocity and vorticity contour plots for the single helix geometries are shown at the top of each figure. For both Reynolds numbers investigated, it is clear that the axial velocity profile throughout helix A is very different to that for $R = 0.2$, and is typical of that in a larger helical radius. In helix B

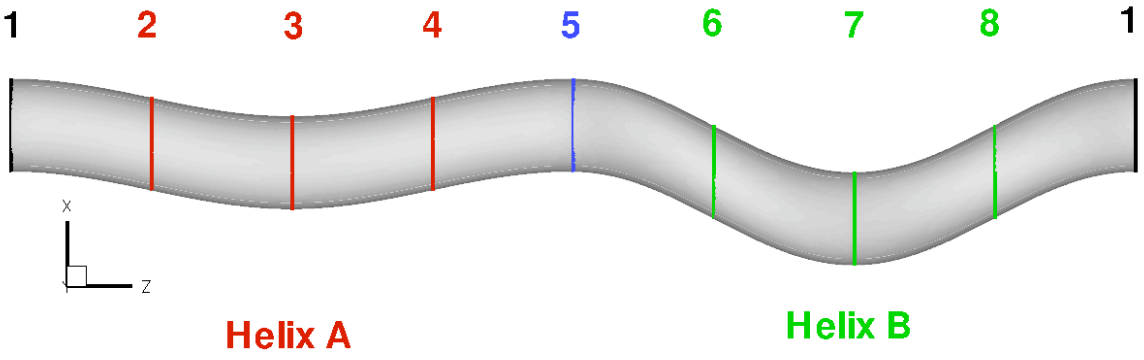


Figure 4: Locations of the slices of the velocity field, shown on geometry $R_A = 0.2D$ and $R_B = 0.5D$

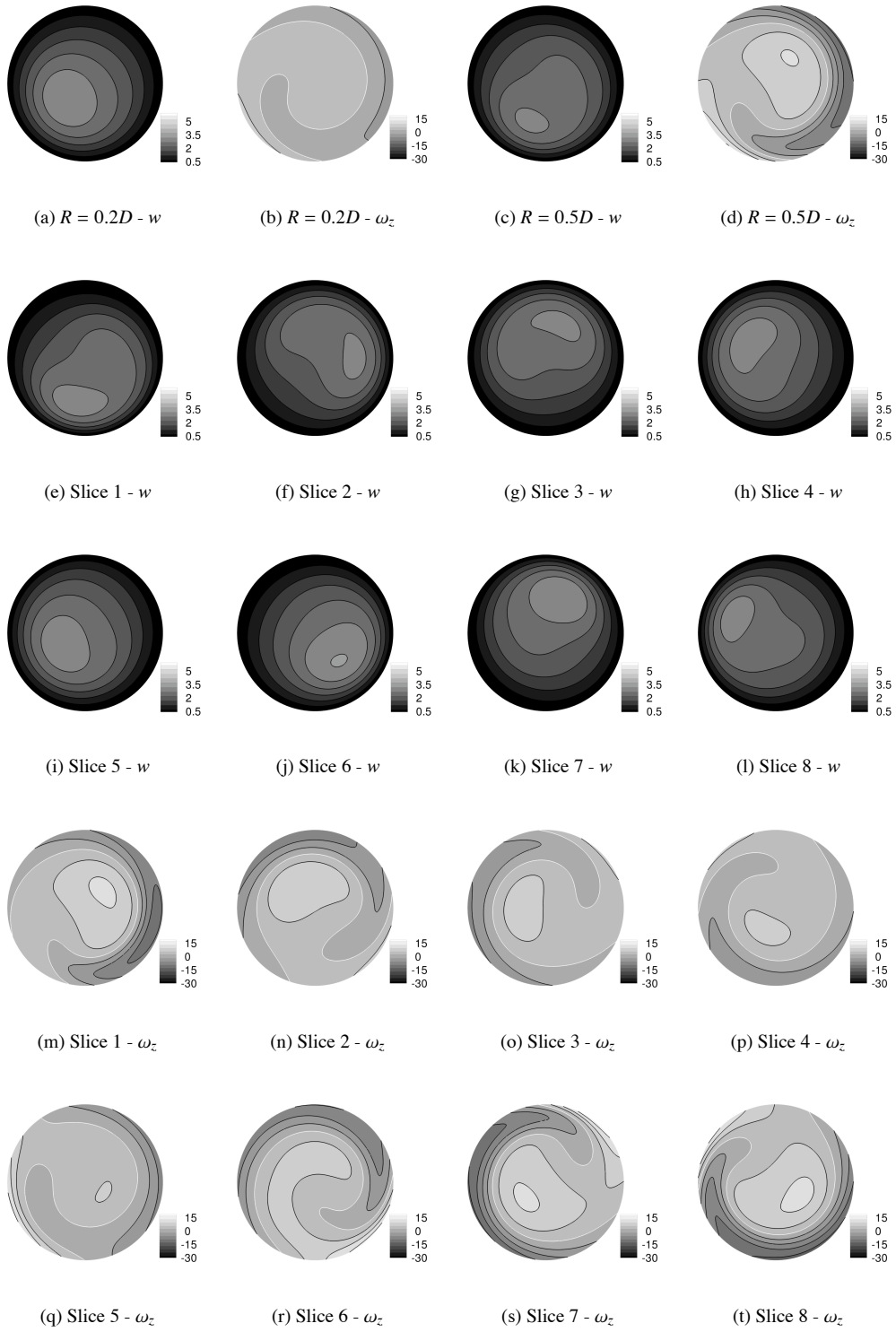
the velocity profile is again different from $R = 0.5$. Examining each slice in sequence, shows that Slice 1 (Figs. 5(e) & 6(e)), which is the outlet of geometry B & the inlet to geometry A, has a velocity profile similar to the single geometry solution, particularly for $R_e = 125$. Slices 2-4 (Figs. 5(f)-5(h) & 6(f)-6(h)) show that the peak value of the axial velocity moves away from the wall, until slice 5 (Figs. 5(i) & 6(i)), which is the outlet of geometry A. The velocity profile here whilst somewhat different to that in geometry B, has still not returned to the single pipe profile in Figure 6(a). Slices 6-8 (Figs. 5(j)-5(l) & 6(j)-6(l)) show the reverse process occurring in helix B, as the flow gradually establishes itself in response to the larger helical radius.

In general, the velocity field that might be expected from two relatively mild helices, a concatenation of the two component fields, with a transition between the two occuring over a quarter pitch length, is not found. Rather, the transition appears to occur over a full pitch length of each helix, without quite reaching the solutions found in the single geometry results. Whilst the vortical structure in the flow remains a single vortex throughout, but grows in strength in helix B, and weakens in helix A, this transition again occurs over a full pitch length. Since the effective in-plane velocity is dependent on both the strength of the vortex, and the radial offset of peak axial velocity, it too will transition across the whole geometry. The differences in the effective in-plane velocity field between each geometry will be reduced, and will change more smoothly, both of which will reduce the degree of mixing from the ideal case. However, it is expected that the combined geometry will produce an improvement in mixing over using a single helical geometry for the equivalent two pitch lengths.

Comparing Figures 5(d) & 5(m) reveals that the vortex in the spline fitted geometry is actually stronger than for the single helix solution. Examining the spline fit shows that the curve is steeper than the corresponding helix, which means that the body force terms will be larger. For $R_e = 125$ this difference appears to be small, and is not thought to affect the results significantly. However, for $R_e = 250$ both the vortex strength, and offset of the axial velocity are clearly indicative of a larger helical radius than is actually used, Figures 6(d) & 6(m).

4. Conclusions

An approach has been presented for solving laminar flow in combined helical pipe geometries, using a coordinate transformation of the Navier-Stokes equations, within a spectral/hp element framework. The preliminary results show that whilst a single vortical structure exists throughout the geometries, its strength varies with axial distance. The change in axial velocity profile is more marked, which is expected to alter the in-plane velocity field more than anticipated, and likewise the mixing behaviour. Specifically the velocity fields never attain their respective single helix solutions, with the flow changing significantly throughout the geometry, vindicating the decision to perform these flow calculations. Furthermore, this methodology can, in principle, be applied to solve the flow in any spline fitted pipe geometry, where the splines are functions only of z, and periodic boundary conditions applies.



(a) $R = 0.2D$ - w (b) $R = 0.2D$ - ω_z (c) $R = 0.5D$ - w (d) $R = 0.5D$ - ω_z

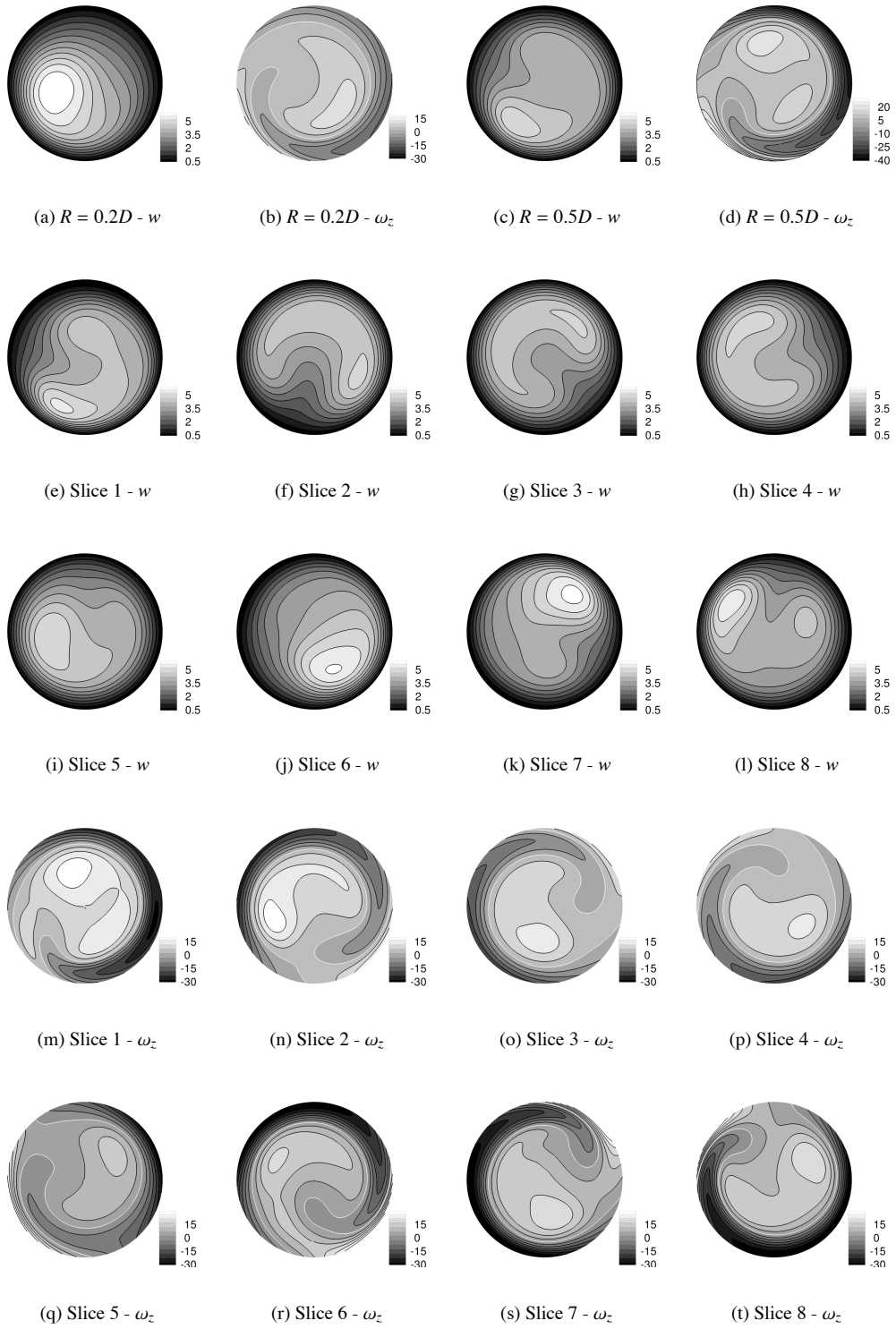
(e) Slice 1 - w (f) Slice 2 - w (g) Slice 3 - w (h) Slice 4 - w

(i) Slice 5 - w (j) Slice 6 - w (k) Slice 7 - w (l) Slice 8 - w

(m) Slice 1 - ω_z (n) Slice 2 - ω_z (o) Slice 3 - ω_z (p) Slice 4 - ω_z

(q) Slice 5 - ω_z (r) Slice 6 - ω_z (s) Slice 7 - ω_z (t) Slice 8 - ω_z

Figure 5: Axial velocity and vorticity contours for case $R_A = 0.2D$ and $R_B = 0.5D$, $R_e = 125$. The zero vorticity contour line is coloured white to highlight the vortical structure



(a) $R = 0.2D$ - w (b) $R = 0.2D$ - ω_z (c) $R = 0.5D$ - w (d) $R = 0.5D$ - ω_z

(e) Slice 1 - w (f) Slice 2 - w (g) Slice 3 - w (h) Slice 4 - w

(i) Slice 5 - w (j) Slice 6 - w (k) Slice 7 - w (l) Slice 8 - w

(m) Slice 1 - ω_z (n) Slice 2 - ω_z (o) Slice 3 - ω_z (p) Slice 4 - ω_z

(q) Slice 5 - ω_z (r) Slice 6 - ω_z (s) Slice 7 - ω_z (t) Slice 8 - ω_z

Figure 6: Axial velocity and vorticity contours for case $R_A = 0.2D$ and $R_B = 0.5D$, $R_e = 250$. The zero vorticity contour line is coloured white to highlight the vortical structure

Acknowledgements

The authors would like to acknowledge Imperial College High Performance Computing Service, *http://www.imperial.ac.uk/ict/services/teachingandresearchservices/highperformancecomputing*, and also EPSRC for providing funding.

References

[1] A. J. Bryan and G. D. Angelini. The biology of saphenous vein graft occlusion: etiology and strategies for prevention. *Current opinion in cardiology*, 9(6), 1994.

[2] C. G. Caro, N. J. Cheshire, and N. Watkins. Preliminary comparative study of small amplitude helical and conventional eptfe arteriovenous shunts in pigs. *Journal of the Royal Society interface*, 2:261–266, 2005.

[3] H. J. T. A. M. Huijbregts, P. J. Blankestijn, C. G. Caro, N. J. W. Cheshire, M. T. C. Hoedt, R. P. Tutein Nolthenius, and F. L. Moll. A helical ptfe arteriovenous access graft to swirl flow across the distal anastomosis: Results of a preliminary clinical study. *European Journal of Vascular and Endovascular Surgery*, 33(4):472–475, 2007.

[4] A. N. Cookson, D. J. Doorly, and S. J. Sherwin. Mixing through stirring of steady flow in small amplitude helical pipes. *Annals of Biomedical Engineering*, under review, 2008.

[5] S. W. Jones, O. M Thomas, and H Aref. Chaotic advection by laminar flow in a twisted pipe. *Journal of Fluid Mechanics*, 209:335–357, 1989.

[6] H. Aref. Stirring by chaotic advection. *Journal of Fluid Mechanics*, 143:1–21, 1984.

[7] D Newman. *A computational study of fluid/structure interactions: flow-induced vibrations of a flexible cable*. PhD thesis, Princeton University, 1996.

[8] W. H. Koberg. *Turbulence control for drag reduction with active wall deformation.* PhD thesis, Imperial College London, 2008.

[9] S. J. Sherwin and G. E. Karnaidakis. *Spectral/hp Element Methods for Computational Fluid Dynamics*. Oxford Science Publications, 2005.